Supplemental Material for "Topological pumping of photons in nonlinear resonator arrays"

J. Tangpanitanon,[1,*] V. M. Bastidas,[1] S. AI-Assam,[2] P. Roushan,[3] D. Jaksch,[2,1] and D. G. Angelakis[1,4]

[1] *Centre for Quantum Technologies, National University of Singapore, 3 Science Drive 2, Singapore 117543*
[2] *Clarendon Laboratory, University of Oxford, Parks Road, Oxford OX1 3PU, United Kingdom*
[3] *Google Inc., Santa Barbara, California 93117, USA*
[4] *School of Electronic and Computer Engineering, Technical University of Crete, Chania, Crete, Greece, 73100*

(Dated: October 22, 2016)

Equations in the main paper are denoted by Eq. [*].

A. Effective three-photon hopping.

In this section, we review the Schrieffer-Wolff (SW) transformation [1] and use it to derive an effective three-photon hopping process. As discussed in the main text, we restrict ourselves to a three-photon manifold of the l-th trimer, i.e. $|300\rangle_l$, $|030\rangle_l$, $|210\rangle_l$ and $|120\rangle_l$. In this subspace, the Hamiltonian is decomposed as

$$H_l = H_l^0 + \lambda V_l, \tag{1}$$

where $H_l^0 = \sum_{m=3l}^{3l-2} \left[\Delta \cos(2\pi m/3 + \phi(t^*)) + n_m(n_m - 1)\right]$ and $\lambda V_l = -J \sum_{m=3l}^{3l-2} \left(a_m^\dagger a_{m+1} + \text{H.c.}\right)$, with $\phi(t^*) = 2\pi/3$.

When $J = 0$, the states $|300\rangle_l$ and $|030\rangle_l$ have the same on-site energy ϵ_3 and so do the states $|210\rangle_l$ and $|120\rangle_l$ with the energy ϵ_2. Hence, the spectrum of H_l^0 can be grouped into two manifolds, labelled as $\mathcal{D}_3 = \{|300\rangle_l, |030\rangle_l\}$ and $\mathcal{D}_2 = \{|210\rangle_l, |120\rangle_l\}$ respectively (see Fig.1). The two manifolds are separated by a gap $\Delta E = \epsilon_2 - \epsilon_3 = -2U$. We consider the hopping term λV_l as a perturbation that couples these manifolds.

Our aim is to find an effective Hamiltonian H_l' which has no matrix elements between the two manifolds. We require that the effective Hamiltonian is related to the original Hamiltonian by a unitary transformation $H_l' = e^{iS^l} H e^{-iS^l}$, where S is a Hermitian matrix. By expanding $S^l = \lambda S_1^l + \lambda^2 S_2^l + \lambda^3 S_3^l + ...$, the effective Hamiltonian can be expressed

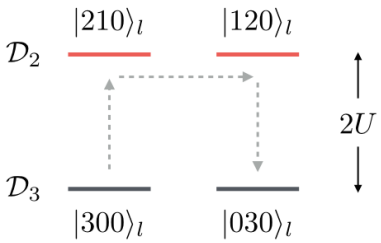

FIG. 1: Diagram showing a third-order three-photon hopping process. For the l-th trimer, the states $|300\rangle_l$ and $|030\rangle_l$ have the same on-site energy as well as $|210\rangle_l$ and $|120\rangle_l$. Hence, they can be grouped into two manifolds, labeled as $\mathcal{D}_3$ and $\mathcal{D}_2$ respectively. The two manifolds are separated by $\Delta E = 2U$. Since the hopping element between $|210\rangle_l$ and $|300\rangle_l$ is $\sqrt{3}J$, we have $\sqrt{3}J/\Delta E < 1$ for $U = J$. This allows a relatively strong third-order hopping process where the three photons hop from $|300\rangle_l$ to $|030\rangle_l$ via the intermediate states $|210\rangle_l$ and $|120\rangle_l$ and vice versa.

*Electronic address: a0122902@u.nus.edu

up to the third order in λ as $H_l' = H_l^0 + H_l'^{(1)} + H_l'^{(2)} + H_l'^{(3)}$, where

$$\begin{aligned}
H_l'^{(1)} =& [\mathrm{i}\lambda S_1^l, H_l^0] + \lambda V_l, \\
H_l'^{(2)} =& [\mathrm{i}\lambda^2 S_2^l, H_l^0] + [\mathrm{i}\lambda S_1^l, \lambda V_l] + \frac{1}{2}[\mathrm{i}\lambda S_1^l, [\mathrm{i}\lambda S_1^l, H_l^0]], \\
H_l'^{(3)} =& [\mathrm{i}\lambda^3 S_3^l, H_l^0] + [\mathrm{i}\lambda^2 S_2^l, \lambda V_l] + \frac{1}{2}[\mathrm{i}\lambda^2 S_2^l, [\mathrm{i}\lambda S_1^l, H_l^0]] + \frac{1}{2}[\mathrm{i}\lambda S_1^l, [\mathrm{i}\lambda^2 (S^l)_2^2, H_l^0]] \\
&+ \frac{1}{2}[\mathrm{i}\lambda S_1^l, [\mathrm{i}\lambda S_1^l, \lambda V_l]] + \frac{1}{6}[\mathrm{i}\lambda S_1^l, [\mathrm{i}\lambda S_1^l, [\mathrm{i}\lambda S_1^l, H_l^0]]].
\end{aligned} \tag{2}$$

Let us consider the first order term $H_l'^{(1)}$. Since the matrix element of H_l' between two manifolds is zero, we have $\langle\alpha|H_l'^{(1)}|\beta\rangle = 0$, where $|\alpha\rangle$ and $|\beta\rangle$ are states from manifolds $\mathcal{D}_\alpha$ and $\mathcal{D}_\beta$ with $\alpha \neq \beta$, respectively. For example, one has that $\langle 300|_l H_l'^{(1)}|210\rangle_l = 0$. However, the S^l matrix that satisfies this condition is not unique. To avoid this, we choose the S^l matrix such that it does not have matrix elements inside each manifold, i.e. $P_\alpha S^l P_\alpha = 0$, for $\alpha \in \{2, 3\}$ where P_α is a projector over the manifold $\mathcal{D}_\alpha$. Therefore, one has $P_2 = |210\rangle_l\langle 210|_l + |120\rangle_l\langle 120|_l$ and $P_3 = |300\rangle_l\langle 300|_l + |030\rangle_l\langle 030|_l$.

With this, the first-order matrix S_1^l can be written as

$$\mathrm{i}\lambda S_1^l = \sum_{\alpha,\beta} \frac{\langle\alpha|\lambda V_l|\beta\rangle}{\epsilon_\beta - \epsilon_\alpha} |\alpha\rangle\langle\beta| = \frac{\sqrt{3}J}{2U} \left(|300\rangle_l\langle 210|_l + |030\rangle\langle 120|_l - h.c.\right). \tag{3}$$

Similarity, since $\langle\alpha|H_l'^{(2)}|\beta\rangle = 0$, the second-order matrix S_2^l is

$$\mathrm{i}\lambda^2 S_2^l = \sum_{\alpha,\beta} \frac{\langle\alpha|[\mathrm{i}\lambda S_1^l, \lambda V_l]|\beta\rangle}{2(\epsilon_\beta - \epsilon_\alpha)} |\alpha\rangle\langle\beta| = \frac{\sqrt{3}J^2}{4\sqrt{2}U^2} \left(|300\rangle_l\langle 120|_l + |030\rangle_l\langle 210|_l - h.c.\right). \tag{4}$$

The third order commutator $[\mathrm{i}\lambda^3 S_3^l, H_l^0]$ is off-diagonal and, by definition, does not contribute to the term $H_l'^{(3)}$. By restricting to the $\mathcal{D}_3$ manifold, i.e. $P_3 H_l' P_3$, the three-photon hopping can be derived from the third-order term as

$$H_{l,J}'^{(3)} = -\frac{J^3}{\sqrt{2}U^2} (|300\rangle_l\langle 030|_l + |030\rangle_l\langle 300|_l). \tag{5}$$

Other terms in $P_3 H_l' P_3$ result in a normalization factor of the on-site energies.

We note that the above scheme is somewhat reminiscent of stimulated Raman adiabatic passage (STIRAP) [2], which employs partially overlapping pulses in time to achieve adiabatic transfer between discrete atomic or molecular quantum states. In contrast, our scheme can be used to transport particles that move adiabatically in a continuous energy band between discrete neighboring lattice sites without dispersion. This is only made possible by the topological properties of the Hamiltonian and results in reliable and robust quantum transport of Fock states in the bulk.

B. Mean field description

To discuss the critical properties of the model Eq. [1], we resort on the mean field analysis [3, 4]. With this aim, we consider a lattice with L sites and periodic boundary conditions $a_0 = a_{L-1}$. We introduce a new set of displaced bosonic operators

$$a_m = b_m + \alpha_m \ , \tag{6}$$

where a_m are the original bosonic operators, and b_m describes the quantum fluctuation about the mean field α_m.

Let us focus now on the particular case of a time independent phase $\phi(t) = \phi_0$ in Eq. [1] and $b = 1/3$. In this particular case, the one dimensional lattice is composed by $L/3$ trimers with on-site energies

$$\begin{aligned}
\omega_A &= \omega_{3l} = \omega_0 + \Delta\cos\phi_0 \\
\omega_B &= \omega_{3l+1} = \omega_0 + \Delta\cos(\phi_0 + 2\pi/3) \\
\omega_C &= \omega_{3l+2} = \omega_0 + \Delta\cos(\phi_0 + 4\pi/3) \ .
\end{aligned} \tag{7}$$

This motivates us to introduce the label $l \in \{0, \ldots, L/3-1\}$ for each unit cell or trimer. Within each trimer one has three species of bosons $b_{A,l} = b_{3l}$, $b_{B,l} = b_{3l+1}$ and $b_{C,l} = b_{3l+2}$ with a similar convention for the mean fields $\alpha_{A,l}$, $\alpha_{B,l}$ and $\alpha_{C,l}$. In the semi-classical limit $|\alpha_m| \gg 1$, one can consider the effect of the quantum fluctuations at a Gaussian level, which enables us to make the decomposition

$$\hat{H}_{\boldsymbol{\alpha}} = \frac{L}{3}\mathcal{H}_{\mathrm{Class}}(\boldsymbol{\alpha}) + \hat{H}_{\mathrm{Lin}}(\boldsymbol{b}, \boldsymbol{\alpha}) + \hat{H}_{\mathrm{Quad}}(\boldsymbol{b}, \boldsymbol{\alpha}) \ , \tag{8}$$

where $\boldsymbol{b} = (b_0, \ldots, b_{L-1})$, and $\boldsymbol{\alpha} = (\alpha_0, \alpha_2, \ldots, \alpha_{L-1})$. The terms $\hat{H}_{\mathrm{Lin}}(\boldsymbol{b}, \boldsymbol{\alpha})$ and $\hat{H}_{\mathrm{Quad}}(\boldsymbol{b}, \boldsymbol{\alpha})$ are linear and quadratic in the bosonic operators, respectively. In addition, if we assume that the mean field do not depend on the position l of the unit cell, we obtain the Hamilton function

$$\begin{aligned}\mathcal{H}_{\mathrm{Class}}(\boldsymbol{\alpha}) =& \omega_A|\alpha_A|^2 + \omega_B|\alpha_B|^2 + \omega_C|\alpha_C|^2 \\ &- J\left(\alpha_A^*\alpha_B + \alpha_B^*\alpha_C + \alpha_C^*\alpha_A + H.c.\right) \\ &+ \frac{U}{2}\left[|\alpha_A|^2(|\alpha_A|^2-1) + |\alpha_B|^2(|\alpha_B|^2-1) + |\alpha_C|^2(|\alpha_C|^2-1)\right] \ .\end{aligned} \tag{9}$$

The quantum fluctuations are governed by the quadratic Hamiltonian

$$\begin{aligned}\hat{H}_{\mathrm{Quad}}(\boldsymbol{a}, \boldsymbol{\alpha}) =& \sum_{m=0}^{L}\left(\omega_m - \frac{U}{2}\right) b_m^\dagger b_m - J\sum_{m=1}^{L-1}\left(b_m^\dagger b_{m+1} + h.c.\right) \\ &+ \frac{U}{2}\sum_{m=0}^{L}\left(|\alpha_m|^2 b_m^\dagger b_m + \alpha_m^2 (b_m^\dagger)^2 + (\alpha_m^*)^2 b_m^2\right) \ ,\end{aligned} \tag{10}$$

where $\alpha_{3l} = \alpha_A$, $\alpha_{3l+1} = \alpha_B$ and $\alpha_{3l+2} = \alpha_C$. One can interpret the Hamiltonian $\hat{H}_{\boldsymbol{\alpha}}$ as the Hamiltonian in neighborhood of a stationary points of the energy landscape Eq. (9). To obtain the stationary points, we require vanishing linear bosonic terms in Eq. (8), i.e., $\hat{H}_{\mathrm{Lin}}(\boldsymbol{a}, \boldsymbol{\alpha}) = 0$. This conditions is satisfied as long as the mean fields α_A, α_B and α_C are a solution of the semi-classical equations of motion. The simplest solution to these equations is $\alpha_A = \alpha_B = \alpha_C = 0$. In this case, the Hamiltonian in Eq. (10) takes a simple form

$$\hat{H}_{\mathrm{Quad}}(\boldsymbol{a}, \boldsymbol{\alpha}) = \sum_{l=0}^{L/3-1} (\boldsymbol{\Psi}_l^\dagger)^{\mathrm{T}} \boldsymbol{\mathcal{M}} \boldsymbol{\Psi}_l + \sum_{l=0}^{L/3-2} J\left[(\boldsymbol{\Psi}_l^\dagger)^{\mathrm{T}} \boldsymbol{\mathcal{N}} \boldsymbol{\Psi}_{l+1} + H.c\right] \ , \tag{11}$$

where $(\boldsymbol{\Psi}_l^\dagger)^{\mathrm{T}} = (b_{A,l}^\dagger, b_{B,l}^\dagger, b_{C,l}^\dagger)$. Correspondingly, the matrices are

$$\boldsymbol{\mathcal{M}} = \begin{pmatrix} \omega_A - U/2 & -J & 0 \\ -J & \omega_B - U/2 & -J \\ 0 & -J & \omega_C - U/2 \end{pmatrix}, \ \boldsymbol{\mathcal{N}} = \begin{pmatrix} 0 & 0 & -J \\ 0 & 0 & 0 \\ -J & 0 & 0 \end{pmatrix} \ . \tag{12}$$

We introduce here a discrete Fourier transformation $\boldsymbol{\Psi}_l = \sqrt{\frac{3}{L}}\sum_k \boldsymbol{\Phi}_k e^{ikl}$, where $(\boldsymbol{\Phi}_k^\dagger)^T = (b_{A,k}^\dagger, b_{B,k}^\dagger, b_{C,k}^\dagger)$, and $b_{\mu,l} = \sqrt{\frac{3}{L}}\sum_k b_{\mu,k} e^{ikl}$ with $\mu \in \{A, B, C\}$. Now we can write Hamiltonian Eq. (11) as $\hat{H}_{\mathrm{Quad}}(\boldsymbol{a}, \boldsymbol{\alpha}) = \sum_k (\boldsymbol{\Phi}_k^\dagger)^T \boldsymbol{H}_k \boldsymbol{\Phi}_k$ with the Bogoliubov de Gennes Hamiltonian

$$\boldsymbol{H}_k = \begin{pmatrix} \omega_A - U/2 & -J & -J\cos k \\ -J & \omega_B - U/2 & -J \\ -J\cos k & -J & \omega_C - U/2 \end{pmatrix} \ . \tag{13}$$

Finally, by considering $U = -J$, and by diagonalizing the Hamiltonian of Eq. (13), one obtains the excitation energies $E_{A,k}$, $E_{B,k}$, and $E_{C,k}$. From this, one can see that when $\omega_A = \omega_B = \omega_C$, we obtain gapless excitations and therefore, a quantum phase transition.

C. Circuit QED implementation

In this section, we review how an array of capacitively-coupled transmon qubits [5] can be mapped to a nonlinear coupled resonator array, as described by the Hamiltonian in Eq. [1]. The derivation provided here can be generalized

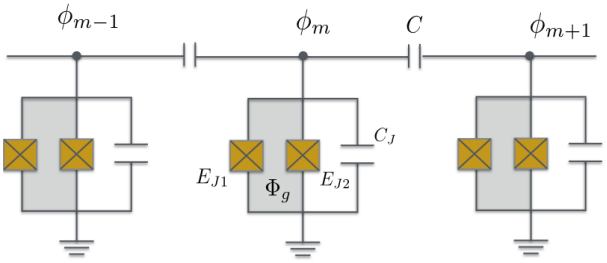

FIG. 2: Circuit diagram implementing the nonlinear coupled resonator array discussed in the main text.

to a more complex coupler such as a transmission line [6–8] and an inductive tunable coupler [9]. Similar approaches have been followed recently in the field of quantum metamaterials where superconducting meta atoms are coupled to photons [10–13].

Our circuit diagram is shown in Fig.2. The flux variable is defined as $\phi_m = -\int V_m dt$, where V_m is a voltage at the corresponding position. As will be shown below, this quantity can be quantized to the form $\phi_m = \alpha(a_m + a_m^\dagger)$, where $a_m, a_m^\dagger$ are bosonic operators of an "artificial" photon at site m and α is some constant that depends on the circuit's elements. As shown in [5], two parallel-connected Josephson junction with a flux bias Φ_g can be thought of as an effective single Josephson junctions E_J where

$$E_J = (E_{J1} + E_{J2}) \cos\left(\frac{\Phi_g}{2\Phi_0}\right) \sqrt{1 + d^2 \tan\left(\frac{\Phi_g}{2\Phi_0}\right)}, \tag{14}$$

with $\Phi_0 = \hbar/2e$ and $d = (E_{J2} - E_{J1})/(E_{J2} + E_{J1})$. The resonator's frequency ω_m is related to E_J, hence it can be tuned on the fly, by changing the flux bias Φ_g.

Following the standard circuit quantization procedure [14], we first write down the circuit's Lagrangian as

$$\mathcal{L} = \sum_{m=0}^{L-1} \left(\frac{1}{2} C_J \dot{\phi}_m^2 + E_J \cos\left(\frac{\phi_m}{\phi_0}\right)\right) + \sum_{m=0}^{L-2} \frac{1}{2} C (\dot{\phi}_m - \dot{\phi}_{m+1})^2, \tag{15}$$

Assuming $C/(C_J + 2C) \ll 1$, the Hamiltonian can be obtained using the Legendre transformation [15],

$$H = \sum_{m=0}^{L-1} \left(\frac{\dot{\phi}_m^2}{2\tilde{C}} + \frac{\phi_m^2}{2\tilde{L}} + \sum_{n=2}^{\infty} \frac{(-1)^n E_J}{(2n)! \Phi_0^{2n}} \phi_m^{2n} \right) + \sum_{m=0}^{L-2} \frac{C}{\tilde{C}^2} q_m q_{m+1}, \tag{16}$$

where $q_m = \sqrt{2C + C_J} \partial \mathcal{L} / \partial \dot{\phi_m}$ is a conjugate momentum of ϕ_m, $\tilde{C} = C_J + 2C$ is an effective capacitance and $\tilde{L} = \Phi_0^2 / E_J$ is an effective inductance . We then quantized ϕ_m and q_m by defining ladder operators a_m, $a_m^\dagger$ according to $\phi_m = (\tilde{L}/4\tilde{C})^{1/4}(a_m + a_m^\dagger)$ and $q_m = i(\tilde{C}/4\tilde{L})^{1/4}(-a_m + a_m^\dagger)$. The first two terms in Eq.16 become $\sum_m \omega a_m^\dagger a_m$, where $\omega = 1/\sqrt{\tilde{L}\tilde{C}}$ is a resonator frequency. In addition, the capacitor C leads to the hopping term with $J = -\frac{\omega C}{2\tilde{C}}$. A rotating-wave approximation is assumed, so we ignore the term $(a_m^\dagger a_{m+1}^\dagger + h.c.)$.

The Josephson junction E_J introduces an anharmonicity to the resonator's frequency. Due to this anharmonicity, a vacuum state $|0\rangle$ and a one-photon Fock state $|1\rangle$ of the resonator can be used as a qubit. A transmon qubit corresponds to the regime with a large $E_{\tilde{L}}/E_{\tilde{C}} > 1$ where $E_{\tilde{C}} = e^2/2\tilde{C}$ and $E_{\tilde{L}} = \Phi_0^2/\tilde{L}$, such that the terms higher than the forth order can be neglected [5]. Hence, a transmon qubit can be thought of as a resonator with an attractive Kerr nonlinearity $U < 0$. Taking into account the normal ordering [6], we get $U = -E_J e^{-\lambda^2} \lambda^4/4$, where $\lambda = (2E_{\tilde{C}}/E_{\tilde{L}})^{1/4}$. This normal ordering also introduces a small normalisation factor $\delta\omega$to the resonator frequency, with $\delta\omega = \lambda^2 E_J e^{-\lambda^2}$.

Note that all Hamiltonian parameters (ω_m, J and U) depend on E_J. Hence, in general, tuning ω also effects other parameters as well. In the main text, we tune the resonator frequency within the range $[\omega_0 - \Delta, \omega_0 + \Delta]$, where $\omega_0 \sim 5$ GHz, $\Delta = 400$ MHz and $J = -U = 40$ MHz. Hence ω_m only changes by $\sim 8\%$. Therefore, subsequent changes in J and U are small compared to Δ and do not alter our discussion in the main text. We also note that using a magnetic flux to drive the Hamiltonian in the MHz timescale has been experimentally realized [16, 17].

D. Numerical Methods

Simulating quantum many-body systems exactly requires resources that grow exponentially with system size, and therefore we use approximate numerical methods. We use the matrix product state (MPS) representation and algorithms [18–20] which have been shown to be very successful for 1D gapped systems. The MPS representation encodes the many-body wave function as a network of order-3 tensors, each possessing two internal indices of maximum dimension χ, and a physical index of dimension $(N_{\max}+1)$ which represents the local Hilbert space. Here, $N_{\max}$ is the maximum number of particles per site. The more entanglement there is in the system the larger χ must be to ensure accurate results.

Based on the MPS representation, we perform time evolution of a pure quantum state using Time-Evolving Block Decimation (TEBD) [21]. For dissipative dynamics, we solve the Lindblad Master equation using quantum trajectories [22]. Since each trajectory is the time evolution of a pure state, the latter can also be performed efficiently within the TEBD framework.

Our implementation of the above methods is based on the open-source Tensor Network Theory (TNT) library [23]. We found that the results shown in the manuscipt can be sufficiently simulated with $\chi = 100$ and $N_{\max} = 4$. Time evolution is discretized in the timestep of $\delta t = 0.02/J$ and for the dissipative dynamics, time evolution of the density matrix is calculated by averaging over $M = 1000$ trajectories. We observed that increasing $\chi, N_{\max}, M$ and reducing δt further do not lead to any significant changes in our results.

[1] C. Cohen-Tannoudji, J. Dupont-Roc, and G. Grynberg, *Atom-Photon interaction: Basic process and application*, Wiley, New York (Chap B1.), 1998.
[2] K. Bergmann, H. Theuer, and B. W. Shore, Rev. Mod. Phys. **70**, 1003 (1998).
[3] N. Lörch, J. Qian, A. Clerk, F. Marquardt, and K. Hammerer, Phys. Rev. X **4**, 011015 (2014).
[4] V. M. Bastidas, I. Omelchenko, A. Zakharova, E. Schöll, and T. Brandes, *Control of Self-Organizing Nonlinear Systems*, chapter Chimera States in Quantum Mechanics, pages 315–336, Springer International Publishing, Cham, 2016.
[5] J. Koch et al., Phys. Rev. A **76**, 042319 (2007).
[6] M. Leib, F. Deppe, A. Marx, R. Gross, and M. J. Hartmann, New Journal of Physics **14**, 075024 (2012).
[7] J. Majer et al., Nature **449**, 443 (2007).
[8] M. A. Sillanpaa, J. I. Park, and R. W. Simmonds, Nature **449**, 438 (2007).
[9] Y. Chen et al., Phys. Rev. Lett. **113**, 220502 (2014).
[10] P. Macha et al., Nature Communications **5**, 5146 EP (2014).
[11] P. Jung, A. V. Ustinov, and S. M. Anlage, Superconductor Science and Technology **27**, 073001 (2014).
[12] V. Pierro and G. Filatrella, Physica C: Superconductivity and its Applications **517**, 37 (2015).
[13] H. R. Mohebbi and A. H. Majedi, IEEE Transactions on Applied Superconductivity **19**, 891 (2009).
[14] M. H. Devoret, Les Houches Session LXIII, Quantum Fluctuations (1995).
[15] A. Nunnenkamp, J. Koch, and S. M. Girvin, New Journal of Physics **13**, 095008 (2011).
[16] P. Roushan et al., arXiv:1606.00077v2 (2016).
[17] R. Barends et al., Nature **508**, 500 (2014).
[18] U. Schollwck, Annals of Physics **326**, 96 (2011), January 2011 Special Issue.
[19] F. Verstraete, V. Murg, and J. Cirac, Advances in Physics **57**, 143 (2008).
[20] R. Ors, Annals of Physics **349**, 117 (2014).
[21] G. Vidal, Phys. Rev. Lett. **91**, 147902 (2003).
[22] A. J. Daley, Advances in Physics , 77 (2014).
[23] S. Al-Assam, S. Clark, D. Jaksch, and TNT Development team, Tensor Network Theory Library, Beta Version 1.1 , www.tensornetworktheory.org, arXiv:1610.02244 (2016).